

Neutrino-induced upward stopping muons in Super-Kamiokande

(February 1, 2020)

The Super-Kamiokande Collaboration

Y.Fukuda^a, K.Ishihara^a, Y.Itow^a, T.Kajita^a, J.Kameda^a, S.Kasuga^a, K.Kobayashi^a, Y.Kobayashi^a, Y.Koshio^a, M.Miura^a, M.Nakahata^a, S.Nakayama^a, Y.Obayashi^a, A.Okada^a, K.Okumura^a, N.Sakurai^a, M.Shiozawa^a, Y.Suzuki^a, H.Takeuchi^a, Y.Takeuchi^a, Y.Totsuka^a, S.Yamada^a, M.Earl^b, A.Habig^b, E.Kearns^b, M.D.Messier^b, K.Scholberg^b, J.L.Stone^b, L.R.Sulak^b, C.W.Walter^b, M.Goldhaber^c, T.Barszczak^d, D.Casper^d, W.Gajewski^d, W.R.Kropp^d, S.Mine^d, L.R.Price^d, M.Smy^d, H.W.Sobel^d, M.R.Vagins^d, K.S.Ganezer^e, W.E.Keig^e, R.W.Ellsworth^f, S.Tasaka^g, A.Kabayashi^h, J.G.Learned^h, S.Matsuno^h, V.J.Stenger^h, D.Takemori^h, T.Ishiiⁱ, H.Ishinoⁱ, T.Kobayashiⁱ, K.Nakamuraⁱ, Y.Oyamaⁱ, A.Sakaiⁱ, M.Sakudaⁱ, O.Sasakiⁱ, S.Echigo^j, M.Kohama^j, A.T.Suzuki^j, T.Inagaki^k, K.Nishikawa^k, T.J.Haines^{l,d}, E.Blaufuss^m, B.K.Kim^m, R.Sanford^m, R.Svoboda^m, M.L.Chenⁿ, J.A.Goodmanⁿ, G.W.Sullivanⁿ, J.Hill^o, C.K.Jung^o, K.Martens^o, C.Mauger^o, C.McGrew^o, E.Sharkey^o, B.Viren^o, C.Yanagisawa^o, W.Doki^p, M.Kirisawa^p, S.Inaba^p, K.Miyano^p, H.Okazawa^p, C.Saji^p, M.Takahashi^p, M.Takahata^p, K.Higuchi^q, Y.Nagashima^q, M.Takita^q, T.Yamaguchi^q, M.Yoshida^q, S.B.Kim^r, M.Etoh^s, A.Hasegawa^s, T.Hasegawa^s, S.Hatakeyama^s, K.Inoue^s, T.Iwamoto^s, M.Koga^s, T.Maruyama^s, H.Ogawa^s, J.Shirai^s, A.Suzuki^s, F.Tsushima^s, M.Koshiba^t, Y.Hatakeyama^u, M.Koike^u, M.Nemoto^u, K.Nishijima^u, H.Fujiyasu^v, T.Futagami^v, Y.Hayato^v, Y.Kanaya^v, K.Kaneyuki^v, Y.Watanabe^v, D.Kielczewska^{w,d,*}, J.S.George^{x,‡}, A.L.Stachyra^x, R.J.Wilkes^x, K.K.Young^{x,†}

^aInstitute for Cosmic Ray Research, University of Tokyo, Tanashi, Tokyo 188-8502, Japan

^bDepartment of Physics, Boston University, Boston, MA 02215, USA

^cPhysics Department, Brookhaven National Laboratory, Upton, NY 11973, USA

^dDepartment of Physics and Astronomy, University of California, Irvine, Irvine, CA 92697-4575, USA

^eDepartment of Physics, California State University, Dominguez Hills, Carson, CA 90747, USA

^fDepartment of Physics, George Mason University, Fairfax, VA 22030, USA

^gDepartment of Physics, Gifu University, Gifu, Gifu 501-1193, Japan

^hDepartment of Physics and Astronomy, University of Hawaii, Honolulu, HI 96822, USA

ⁱInst. of Particle and Nuclear Studies, High Energy Accelerator Research Org. (KEK), Tsukuba, Ibaraki 305-0801, Japan

^jDepartment of Physics, Kobe University, Kobe, Hyogo 657-8501, Japan

^kDepartment of Physics, Kyoto University, Kyoto 606-8502, Japan

^lPhysics Division, P-23, Los Alamos National Laboratory, Los Alamos, NM 87544, USA

^mDepartment of Physics and Astronomy, Louisiana State University, Baton Rouge, LA 70803, USA

ⁿDepartment of Physics, University of Maryland, College Park, MD 20742, USA

^oDepartment of Physics and Astronomy, State University of New York, Stony Brook, NY 11794-3800, USA

^pDepartment of Physics, Niigata University, Niigata, Niigata 950-2181, Japan

^qDepartment of Physics, Osaka University, Toyonaka, Osaka 560-0043, Japan

^rDepartment of Physics, Seoul National University, Seoul 151-742, Korea

^sDepartment of Physics, Tohoku University, Sendai, Miyagi 980-8578, Japan

^tThe University of Tokyo, Tokyo 113-0033, Japan

^uDepartment of Physics, Tokai University, Hiratsuka, Kanagawa 259-1292, Japan

^vDepartment of Physics, Tokyo Institute for Technology, Meguro, Tokyo 152-8551, Japan

^wInstitute of Experimental Physics, Warsaw University, 00-681 Warsaw, Poland

^xDepartment of Physics, University of Washington, Seattle, WA 98195-1560, USA

A total of 137 upward stopping muons of minimum energy 1.6 GeV are observed by Super-Kamiokande during 516 detector live days. The measured muon flux is $0.39 \pm 0.04(\text{stat.}) \pm 0.02(\text{syst.}) \times 10^{-13} \text{cm}^{-2}\text{s}^{-1}\text{sr}^{-1}$ compared to an expected flux of $0.73 \pm 0.16(\text{theo.}) \times 10^{-13} \text{cm}^{-2}\text{s}^{-1}\text{sr}^{-1}$. Using our previously-published measurement of the upward through-going muon flux, we calculate the stopping/through-going flux ratio \mathcal{R} , which has less theoretical uncertainty. The measured value of $\mathcal{R} = 0.22 \pm 0.02(\text{stat.}) \pm 0.01(\text{syst.})$ is significantly smaller than the value $0.37^{+0.05}_{-0.04}(\text{theo.})$ expected using the best theoretical information (the probability that the measured \mathcal{R} is a statistical fluctuation below the expected value is 0.39%). A simultaneous fitting to zenith angle distributions of upward stopping and through-going muons gives a result which is consistent with the hypothesis of neutrino oscillations with the parameters $\sin^2 2\theta > 0.7$ and $1.5 \times 10^{-3} < \Delta m^2 < 1.5 \times 10^{-2} \text{ eV}^2$ at 90% confidence level, providing a confirmation of the observation of neutrino oscillations by Super-Kamiokande using the contained atmospheric neutrino events.

PACS numbers: 14.60.Pq, 96.40.Tv

keywords: *neutrino oscillations, Super-Kamiokande, upward stopping muons, upward throughgoing muons, atmospheric muon neutrinos, cosmic rays*

Energetic atmospheric ν_μ or $\bar{\nu}_\mu$ interact with the rock surrounding the Super-Kamiokande (“Super-K”) detector and produce muons via weak interactions. For downward-going particles, the rock overburden is insufficient to prevent cosmic-ray muons from overwhelming any neutrino induced muons, but upward-going muons are ν_μ or $\bar{\nu}_\mu$ induced because the entire thickness of the earth shields the detector. Muons energetic enough to cross the entire detector are defined as “upward through-going muons”, and have been discussed in a previous article [1]. The typical energy of the parent neutrinos is approximately 100 GeV. Upward-going muons that stop in the detector are defined as “upward stopping muons”, and come from parent atmospheric neutrinos with a typical energy of about 10 GeV. These energy spectra are shown in Fig. 1. Neutrinos arriving vertically from beneath the detector travel roughly 13,000 km from their point of production, while those coming from near the horizon originate only \sim 500 km away. Thus, observation of upward-going muons provides a relatively pure sample of muon neutrinos, with a wide range of path lengths, allowing tests of possible ν_μ disappearance due to flavor neutrino oscillations [2].

For atmospheric neutrinos with interaction vertices inside the detector’s fiducial volume (referred to as “contained” events), Super-K measures a low ν_μ/ν_e ratio [3] and clearly observes a strong zenith angle dependence of the ν_μ events [4]. This muon neutrino disappearance [5] is consistent with $\nu_\mu \leftrightarrow \nu_\tau$ oscillations, while the up-down symmetry seen in the ν_e events rules out significant ν_e appearance, in agreement with recent results from the CHOOZ experiment [6]. The $\nu_\mu \leftrightarrow \nu_\tau$ oscillation hypothesis suggested to explain the Super-K contained event results is also consistent with anomalous upward through-going muon zenith angle distributions observed by Kamiokande [7], MACRO [8] and Super-Kamiokande [1]. The upward stopping muons are the remaining class of atmospheric neutrino events with which Super-K can test the oscillation hypothesis. It should be noted here that the parent neutrino energies of upward stopping muons are similar to those of multi-GeV fully-contained (FC) and partially-contained (PC) events discussed in [4]. Thus, a similar deficit of upward stopping muons to that of upward-going multi-GeV FC and PC events is expected if the oscillation hypothesis is the cause of the multi-GeV FC and PC event deficit. The main difference between the multi-GeV FC and PC event sample and the upward stopping muon sample is that roughly 80% of the upward stopping muons are generated in the surrounding rock, which has different neutrino interaction cross-sections and systematic uncertainties than does water.

The Super-K detector is a 50 kton cylindrical water Cherenkov detector. To reduce the cosmic-ray muon background, the detector was constructed \sim 1000 m (2700 m.w.e.) underground at the Kamioka Observatory, Institute for Cosmic Ray Research, the University of Tokyo, in the Kamioka-Mozumi mine, Japan. The detector is divided by an optical barrier instrumented with photomultiplier tubes (“PMT”s) into a cylindrical primary detector region (the Inner Detector, or “ID”) and a surrounding shell of water (the Outer Detector, or “OD”) serving as a cosmic-ray veto counter. Details of the detector and general data reduction procedures can be found in reference [3]. The data used in this analysis were taken from Apr. 1996 to Jan. 1998, corresponding to 516 days of detector livetime.

An upward-going muon is defined as a track that appears to enter the detector from the rock, and reconstructs as traveling in the upward direction. Thus, PMT activity in the OD at the muon’s entrance point is required. The total cosmic-ray muon rate at Super-K is 2.2 Hz, of which a few percent are stopping muons, and the great majority are downward-going. The trigger efficiency for a muon entering the ID with momentum more than 200 MeV/c is \sim 100% for all zenith angles.

Muons which leave entrance signal clusters in the OD with no corresponding exit cluster are regarded as stopping. A neutrino interaction inside the water of the OD also produces such a signal, so some fraction (\sim 20%) of the upward-going stopping muon sample is estimated to originate in the OD rather than the rock according to simulations. This effect has been accounted for in the expected flux calculations.

Stopping muons with track length > 7 m (\sim 1.6 GeV) in the ID are selected for further analysis. The stopping muon track length is determined by calculating the muon momentum from a photoelectron count in the same way as in the contained event analysis [3]. This cut eliminates short tracks that are very close to the PMTs and thus are hard to reconstruct, provides an energy threshold, and also eliminates nearly all contamination of the upward stopping muon signal by pions. These pions are photoproduced by cosmic-ray muons outside the detector and are observed to have a soft spectrum [9], such that residual contamination upward-going pions meeting the 7 m track length requirement is estimated to be $< 1\%$. The nominal detector effective area for upward-going muons with a track length > 7 m in the ID is \sim 1200 m².

137 upward stopping muons which satisfy a $\cos \Theta < 0$ cut are found, where Θ is the zenith angle of the muon track, with $\cos \Theta = -1$ corresponding to vertically upward-going events.

Details of the muon track reconstruction method and data reduction algorithm are similar to those of through-going muons described elsewhere [1]. The total detection efficiency for the complete data reduction process for upward stopping muons is estimated by a Monte Carlo simulation to be >98% over $-1 < \cos \Theta < 0$. The validity of this Monte Carlo estimate is in turn checked with real cosmic-ray downward stopping muons, taking advantage of the up/down symmetry of the detector geometry.

Because of multiple Coulomb scattering and finite muon fitter angular resolution ($\sim 1^\circ$ [1]), some of the abundant downward-going cosmic-ray stopping muon background may be reconstructed with $\cos \Theta < 0$ and contaminate the neutrino induced upward stopping muon sample. Figure 2 illustrates the estimation of this contamination by extrapolation of the downward-going zenith angle distribution to the flat neutrino-induced signal near the horizon. This background falls exponentially with decreasing $\cos \Theta$, the contribution to apparent upward stopping muons is estimated to be 10.8 ± 4.2 events in the zenith angle bin with $\cos \Theta$ between -0.2 and 0. This is a larger contamination than was present in the upward through-going muon sample due to the lower muon energies (and correspondingly larger multiple scattering) of the stopping muon sample, and is more uncertain due to lower statistics. As an independent crosscheck of the background contamination, the energy spectrum of the observed stopping muons is shown in Fig. 3. That shape is consistent with the expected and no significant contamination is observed at the 1.6 GeV muon energy analysis threshold.

To analytically calculate the expected upward stopping (and through-going as well) muon flux, employed is the combination of the Bartol atmospheric neutrino flux model [10], a neutrino interaction model composed of quasi-elastic (QE) scattering [11] + single-pion (1π) production [12] + deep inelastic (DIS) scattering multi-pion production based on the parton distribution functions (PDF) of GRV94 [13] with the additional kinematic constraint of $W > 1.4 \text{ GeV}/c^2$ (where W is the invariant mass of the hadronic recoil system), and Lohmann's muon energy loss formula in standard rock [14].

This expected flux is compared to three other analytic calculations to estimate the model-dependent uncertainties of the expected muon flux. The other flux calculations use various pairwise permutations of the Honda flux [15] or the atmospheric neutrino flux model calculated by the Bartol group [10], the GRV94DIS PDF or the CTEQ3M [16]PDF. This comparison yields $\pm 10\%$ of difference in the overall flux and -2% to +1% for the bin-by-bin shape difference in the zenith-angle distribution. The shape difference is due mostly to differences in the input flux models.

The expected muon flux $\Phi_{\text{theo}}^{\text{stop}}$ resulting from the above calculation is $0.73 \pm 0.16 \times 10^{-13} \text{ cm}^{-2} \text{ s}^{-1} \text{ sr}^{-1}$ ($\cos \Theta < 0$), where the estimated theoretical uncertainties are described in Table I. The dominant error comes from the overall normalization uncertainty in the neutrino flux, which is estimated to be approximately $\pm 20\%$ [10,15,17] above several GeV.

Given the detector live time T , the effective area for upward stopping muons $S(\Theta)$, and the detection efficiency $\varepsilon(\Theta)$, the upward stopping muon flux is calculated using:

$$\Phi^{\text{stop}} = \sum_{j=1}^N \frac{1}{\varepsilon(\Theta_j)} \cdot \frac{1}{S(\Theta_j) 2\pi} \cdot \frac{1}{T}$$

where the index j runs over observed events, 2π is the total solid angle covered by the detector for upward stopping muons, and N is the total number of observed muon events (137). Subsequently, we subtract the cosmic-ray muon contamination (10.8 events) from the most horizontal bin ($-0.2 < \cos \Theta < 0$). The resulting observed upward stopping muon flux is: $\Phi^{\text{stop}} = 0.39 \pm 0.04(\text{stat.}) \pm 0.02(\text{sys.}) \times 10^{-13} \text{ cm}^{-2} \text{ s}^{-1} \text{ sr}^{-1}$. If instead of subtracting this background, we simply omit upward stopping muons coming from the thin-rock region [1] in the most horizontal $\cos \Theta$ bin ($-0.1 < \cos \Theta < 0$ and $60^\circ < \phi < 310^\circ$), the calculated flux differs from the background-subtracted flux by -1.1%. Systematic errors in the experimental measurement are summarized in Table II.

The flux as a function of zenith angle, ($d\Phi^{\text{stop}}/d\Omega$), is shown in Fig. 4. Due to limited statistics for stopping muons, 5 angular bins are used instead of the 10 bins used for Super-K through-going muons. With the present statistics, the shape of the normalized distribution is consistent with the no-oscillations hypothesis ($\chi^2/\text{d.o.f.} = 4.1/4$ corresponding to 39% probability). However, the overall flux of upward stopping muons observed is substantially depressed from that expected, as this shape comparison is made

after multiplying the expected flux by a free-running overall normalization factor $(1+\alpha)$ whose best fit value is $\alpha = -51\%$ calculated by a χ^2 shape fit. This can be compared with an observed no-oscillations $\alpha = -14\%$ in the through-going muon sample [1].

Adding the upward through-going flux [1] Φ^{thru} , we obtain a detector-independent total upward-going muon flux $\Phi^{stop+thru}$ of $2.13 \pm 0.08(\text{stat.}) \pm 0.03(\text{sys.}) \times 10^{-13} \text{cm}^{-2} \text{s}^{-1} \text{sr}^{-1}$ with muon energy $> 1.6 \text{ GeV}$. The zenith angle distribution of the summed flux, $(d\Phi^{stop+thru}/d\Omega)$, is shown in Fig. 5.

A more useful physical quantity than the absolute flux for probing neutrino oscillations is the stopping/through-going flux ratio $\mathcal{R} = \Phi^{stop}/\Phi^{thru}$, which cancels much of the large ($\sim 20\%$) uncertainty in the neutrino flux normalization and the neutrino interaction cross sections [18]. The systematic theoretical and experimental uncertainties in \mathcal{R} are summarized in Table III and Table IV, respectively. The measured \mathcal{R} is $0.22 \pm 0.02(\text{stat.}) \pm 0.01(\text{sys.})$, while the expected $\mathcal{R}_{\text{theo}}$ is $0.37^{+0.05}_{-0.04}(\text{theo.})$. The probability that the observed ratio could fluctuate this far below the expectation is 0.39%. The zenith angle distribution of the ratio \mathcal{R} is shown in Fig. 6.

Using these data, we derive probability contours on the neutrino oscillation parameter $(\sin^2 2\theta, \Delta m^2)$ plane for the $\nu_\mu \leftrightarrow \nu_\tau$ oscillation hypothesis, as shown in Fig. 7, based on a χ^2 defined by:

$$\chi^2 = \min_{\beta} \left[\sum_{i=1}^{5(\text{stop})} \left(\frac{\mathcal{R}^i - \mathcal{R}_{\text{theo}}^i(\sin^2 2\theta, \Delta m^2) \times (1 + \beta)}{\sqrt{\sigma_{\mathcal{R}_{\text{stat}}^i}^2 + \sigma_{\mathcal{R}_{\text{sys}}^i}^2}} \right)^2 + \left(\frac{\beta}{\sigma_\beta} \right)^2 \right]$$

where \mathcal{R}^i is the observed ratio in the i -th $\cos\Theta$ bin, $\sigma_{\mathcal{R}_{\text{stat}}^i}$ the experimental statistical error, $\sigma_{\mathcal{R}_{\text{sys}}^i}$ the bin-by-bin uncorrelated systematic error ($\simeq 2\%$) estimated by adding uncorrelated theoretical and experimental systematic errors in Table III and Table IV in quadrature, and $\mathcal{R}_{\text{theo}}^i$ the expected ratio. The β for $\mathcal{R}_{\text{theo}}^i$ represents a stopping-to-throughgoing relative muon flux normalization factor with error $\sigma_\beta = 14\%$ estimated by the correlated theoretical and experimental systematic errors in Table III and Table IV added in quadrature.

The allowed region thus obtained in Fig. 7 is in good agreement with that found in the Super-K contained event analysis [5]. The minimum χ^2 locations on the $\Delta m^2 - \sin^2 2\theta$ plane and corresponding parameter values for various conditions are listed in Table V. As the minimum χ^2 lies in the unphysical region, the contour is drawn according to the prescription for bounded physical regions given in Ref. [19]. Because the χ^2 surface has a rather broad minimum, the specific best-fit oscillation parameter values cited are of less importance than the contours shown in Fig. 7. If we replace the Bartol neutrino flux [10] by the Honda's flux [15] and/or the GRV94DIS parton distribution functions [13] by CTEQ3M [16], the allowed region contours do not change significantly.

Finally, we performed an oscillation analysis which use all the upward-going muon information available by simultaneously fitting to the upward through-going and stopping muon zenith angle distributions. In this analysis, χ^2 is defined by the sum over 10 upward-throughgoing and 5 upward-stopping muon zenith angle bins:

$$\chi^2 = \min_{\alpha, \beta} \left[\sum_{i=1}^{10(\text{thru})} \left(\frac{\left(\frac{d\Phi}{d\Omega} \right)^i - (1 + \alpha) \left(\frac{d\Phi}{d\Omega} \right)_{\text{theo}}^i(\sin^2 2\theta, \Delta m^2)}{\sqrt{(\sigma_{\text{stat}}^i)^2 + (\sigma_{\text{sys}}^i)^2}} \right)^2 + \sum_{i=1}^{5(\text{stop})} \left(\frac{\left(\frac{d\Phi}{d\Omega} \right)^i - (1 + \alpha)(1 + \beta) \left(\frac{d\Phi}{d\Omega} \right)_{\text{theo}}^i(\sin^2 2\theta, \Delta m^2)}{\sqrt{(\sigma_{\text{stat}}^i)^2 + (\sigma_{\text{sys}}^i)^2}} \right)^2 + \left(\frac{\alpha}{\sigma_\alpha} \right)^2 + \left(\frac{\beta}{\sigma_\beta} \right)^2 \right]$$

where $\left(\frac{d\Phi}{d\Omega} \right)^i$ is the observed muon flux in the i -th $\cos\Theta$ bin, σ_{stat}^i the experimental statistical error, σ_{sys}^i (~ 2 to $\sim 4\%$) the bin-by-bin uncorrelated theoretical and experimental systematic errors in Table I and

Table II added in quadrature for *stop* or from Ref. [1] for *thru* , $(\frac{d\Phi}{d\Omega})_{theo}^i$ the expected muon flux, α the running overall flux normalization factor with error σ_α of 22% estimated by adding in quadrature the correlated theoretical systematic errors in Table I, β the running stopping-to-throughgoing relative muon flux normalization factor with error $\sigma_\beta=14\%$ estimated by the correlated theoretical and experimental systematic errors in Table III and Table IV added in quadrature. The results are shown in Fig. 7 and are consistent with those from the Super-K contained event analysis. As is shown in Table V, the minimum χ^2 falls in the unphysical region so the contours are drawn according to the prescription for bounded physical regions given in Ref. [19].

The contamination due to ν_e charged current interactions and neutral current interactions in the upward-going muons is estimated to be < 1% by a Monte Carlo simulation and is neglected in these analyses. The contribution of possible ν_τ interactions in the rock below to the upward stopping muon flux is suppressed by branching ratios and kinematics to less than a few percent, and is also neglected.

The observed overall upward stopping muon flux alone and its zenith angle distribution do not conflict with the expected no-oscillations values significantly within the present statistical and systematic errors. However, in order to simultaneously explain both the stopping and through-going upward muon fluxes using both an analysis based on the stop/through ratio \mathcal{R} and a combined fit of upward stopping and through-going muon zenith angle data, the no-oscillations theoretical expectations reproduce the observed fluxes poorly at the 0.39% C.L. (stop/thru ratio averaged over zenith angle) and 0.87% C.L., respectively, while the $\nu_\mu \leftrightarrow \nu_\tau$ oscillation assumption is consistent with observations. This result supports the evidence for neutrino oscillations given by the analysis of the contained and through-going muon atmospheric neutrino events by Super-K.

We gratefully acknowledge the cooperation of the Kamioka Mining and Smelting Company. The Super-Kamiokande experiment has been built and operated from funding by the Japanese Ministry of Education, Science, Sports and Culture, and the United States Department of Energy.

TABLE I. List of theoretical uncertainties in upward stopping muon flux calculation.

Error source	Error
typical ν flux normalization	$\pm 20\%^a$
Choice of ν flux/PDF	
overall flux	$\pm 10\%^a$
bin by bin	$-2\% \text{ to } +1\%^b$

^aTheoretical $\cos\Theta$ bin-by-bin correlated uncertainty

^bTheoretical $\cos\Theta$ bin-by-bin uncorrelated uncertainty

TABLE II. List of experimental systematic errors in upward stopping muon flux measurement.

Error source	Error
7 m track length cut	$\pm 5\%^a$
Live time	$\pm 1\%^a$
Reconstruction efficiency	$\sim \pm 1\%^b$

^aExperimental $\cos\Theta$ bin-by-bin correlated systematic error

^bExperimental $\cos\Theta$ bin-by-bin uncorrelated systematic error

Note that the uncertainty of the background subtraction is included in the statistical error.

TABLE III. List of theoretical uncertainties in stopping/through-going muon flux ratio.

Error source	Error
Primary spectral index ± 0.05	$\pm 13\%^a$
Choice of ν flux	
overall ratio	$\pm 1\%^a$
bin by bin	$-1\% \text{ to } +2\%^b$
ν cross section ^c	$\pm 4\%^a$

^aTheoretical $\cos\Theta$ bin-by-bin correlated uncertainty

^bTheoretical $\cos\Theta$ bin-by-bin uncorrelated uncertainty

^cQE, 1π and DIS cross sections are changed independently by $\pm 15\%$, and the effect of this on \mathcal{R} is noted here.

TABLE IV. List of experimental systematic errors in stopping/through-going muon flux ratio.

Error source	Error
7 m track length cut	$\pm 5\%^a$
Live time	$\pm 1\%^a$
stop/thru misidentification	$\sim \pm 1\%^a$
Reconstruction efficiency	$\sim \pm 1\%^b$

^aExperimental $\cos\Theta$ -bin-by-bin correlated error

^bExperimental $\cos\Theta$ -bin-by-bin uncorrelated error

 TABLE V. Summary of fit results. See text for definitions of α and β .

Case	Δm^2	$\sin^2 2\theta$	α	β	χ^2_{MIN}/DOF	Probability
Flux vs. zenith angle (Fig. 4):	-	-	-0.51	-	4.1/4	39%
\mathcal{R} analysis (Fig. 6):						
Fit in the physical region	$3.1 \times 10^{-3} \text{ eV}^2$	1.00	-	-0.084	0.76/3	86%
Fit over all space	$3.9 \times 10^{-3} \text{ eV}^2$	1.19	-	-0.003	0.30/3	96%
No oscillations	-	-	-	-0.35	8.4/5	13%
(stop+through) $\cos(\Theta)$ analysis (Fig. 7):						
Fit in the physical region	$3.9 \times 10^{-3} \text{ eV}^2$	1.00	0.061	-0.083	8.8/13	79%
Fit over all space	$3.9 \times 10^{-3} \text{ eV}^2$	1.13	0.10	-0.012	8.2/13	83%
No oscillations	-	-	-0.16	-0.36	31.0/15	0.87%

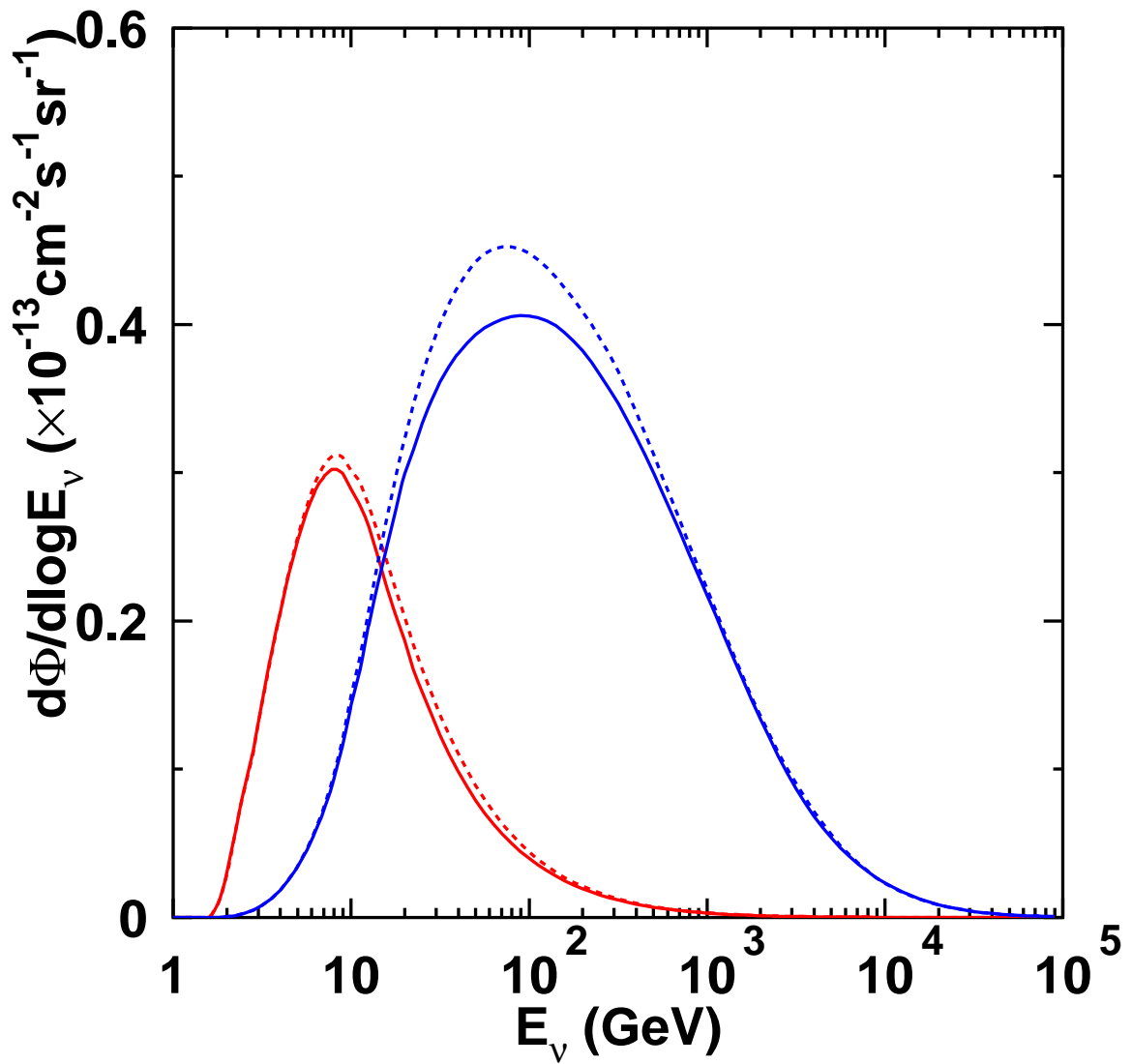


FIG. 1. The energy spectra of the parent neutrinos of upward stopping muons (left) and upward through-going muons (right). The dashed lines are the result of using the Bartol input fluxes, and the solid lines are from Honda's calculations.

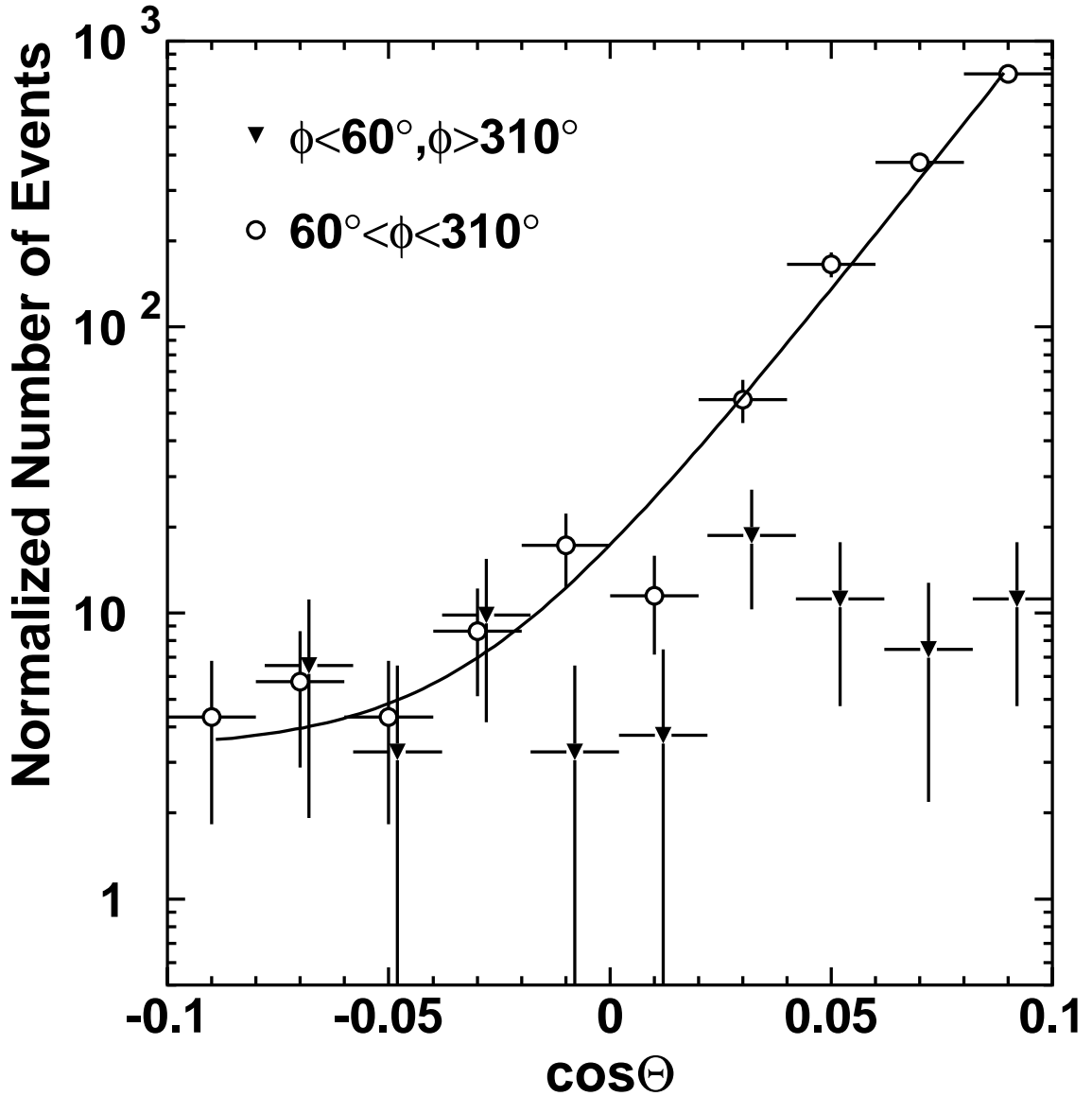


FIG. 2. Zenith angle distribution of stopping muons near the horizon observed by Super-K. Filled triangles (open circles) indicate events coming from direction where the rock overburden is thick > 15000 m.w.e. (shallow > 5000 m.w.e.). The two distributions are normalized to a common azimuth angle range (0 - 360 degrees). The solid line is the zenith fit to the shallow rock events used to estimate the cosmic-ray muon background contamination in the $-0.2 < \cos \Theta < 0$ bin.

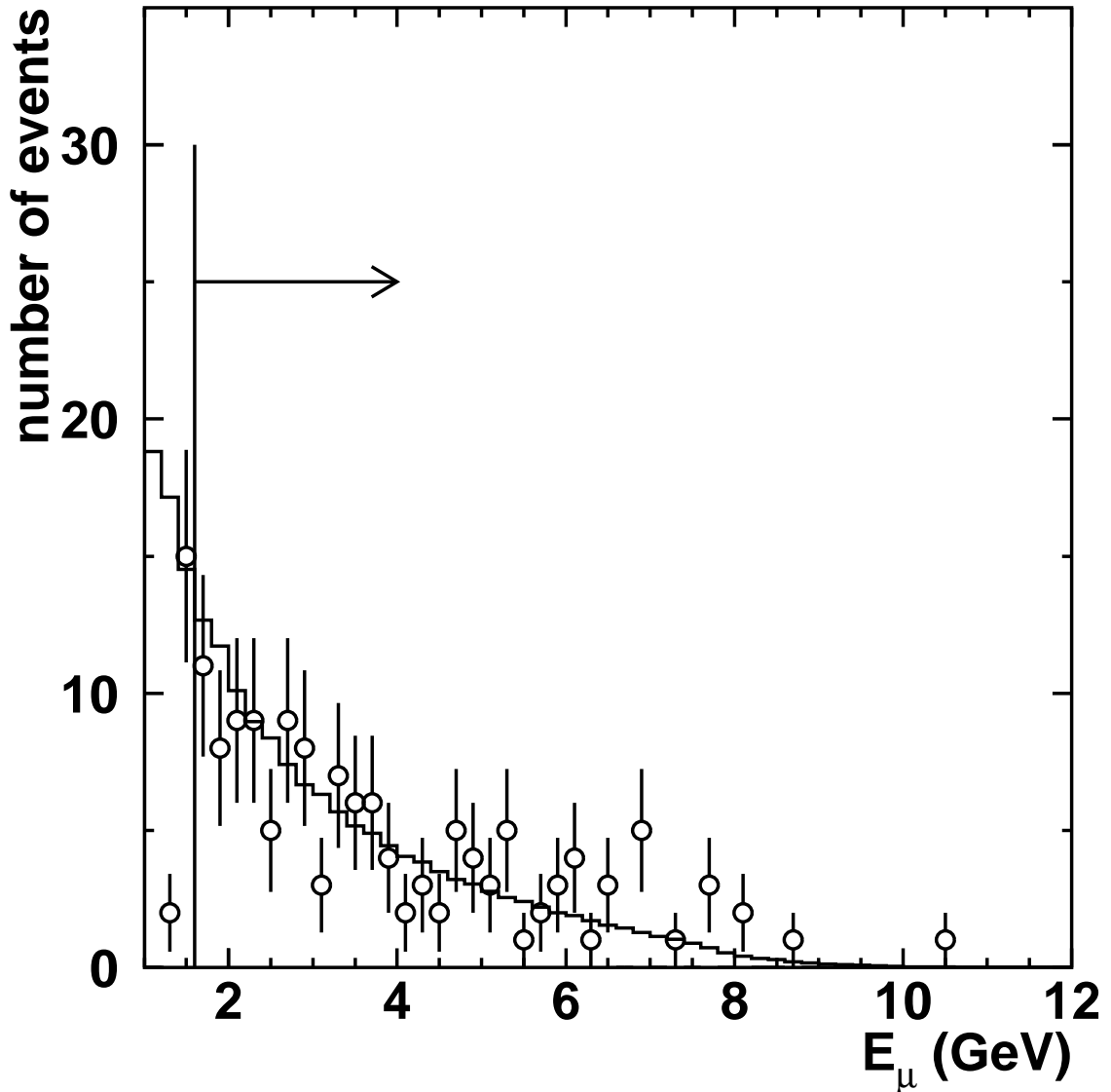


FIG. 3. The energy distribution of upward stopping muons, illustrating the freedom of the data both from threshold effects due to the 7 m (1.6 GeV) muon pathlength cut and from upward-scattered low energy stopping cosmic-ray muons. The solid histogram is the normalized distribution expected from the no-oscillations hypothesis. The normalization is made so that the integrated number of expected events with muon energy > 1.6 GeV (the vertical line) corresponds to the observed number of events (=137). Preselection is applied at muon energy ~ 1.4 GeV.

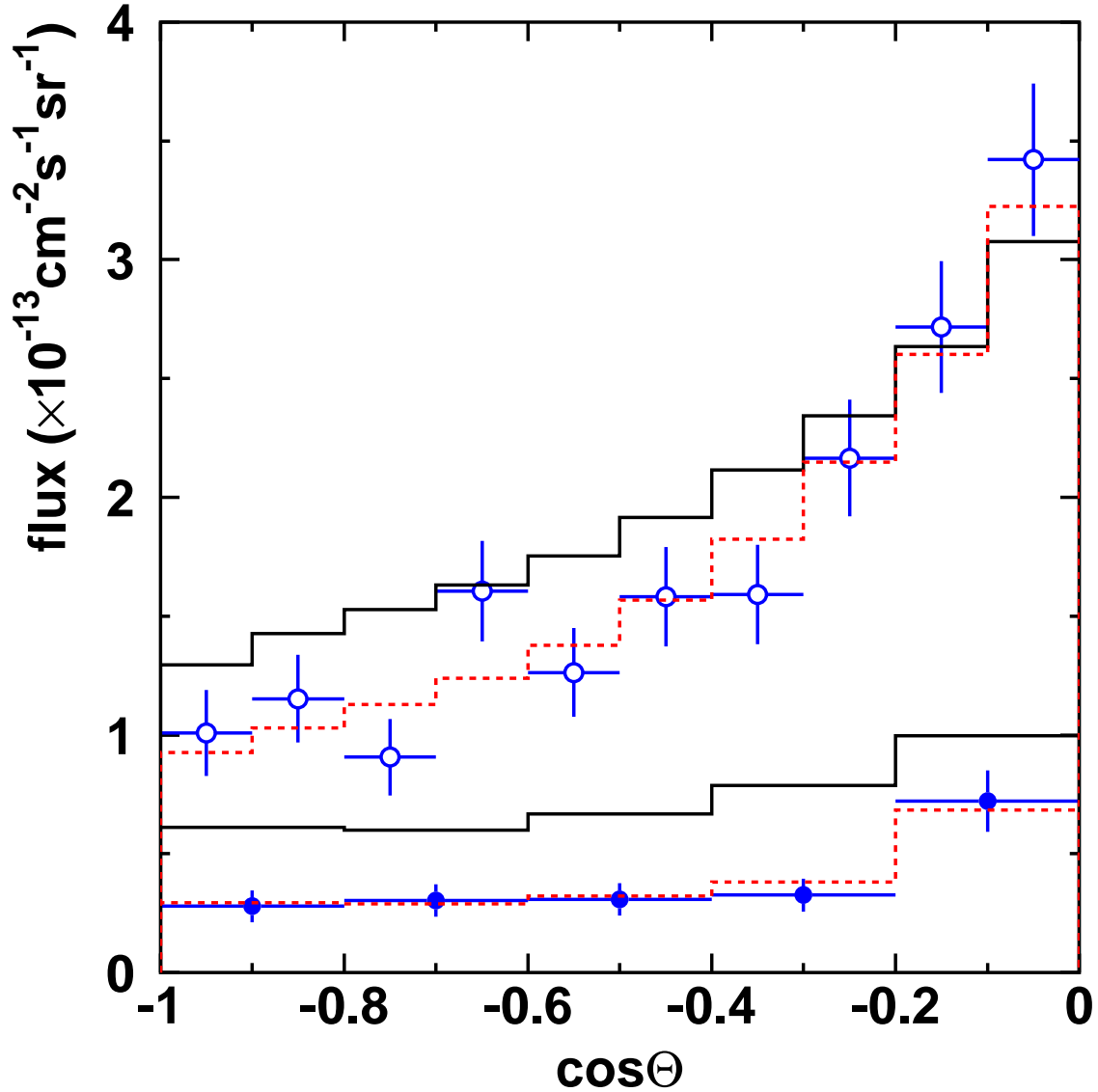


FIG. 4. Upward stopping (filled circles) and through-going (open circles) muon fluxes observed in Super-K as a function of zenith angle. The error bars indicate uncorrelated experimental systematic plus statistical errors added in quadrature. The lower (upper) solid histograms show the expected upward stopping (through-going) muon flux based on the Bartol neutrino flux without oscillation. Also shown as lower (upper) dashed histograms are the expected stopping (through-going) muon flux assuming the best fit parameters of the combined analysis in the physical region at $(\sin^2 2\theta, \Delta m^2) = (1.0, 3.9 \times 10^{-3} \text{ eV}^2)$, $\alpha = +0.061$ and $\beta = -0.083$ for the $\nu_\mu \leftrightarrow \nu_\tau$ oscillation case.

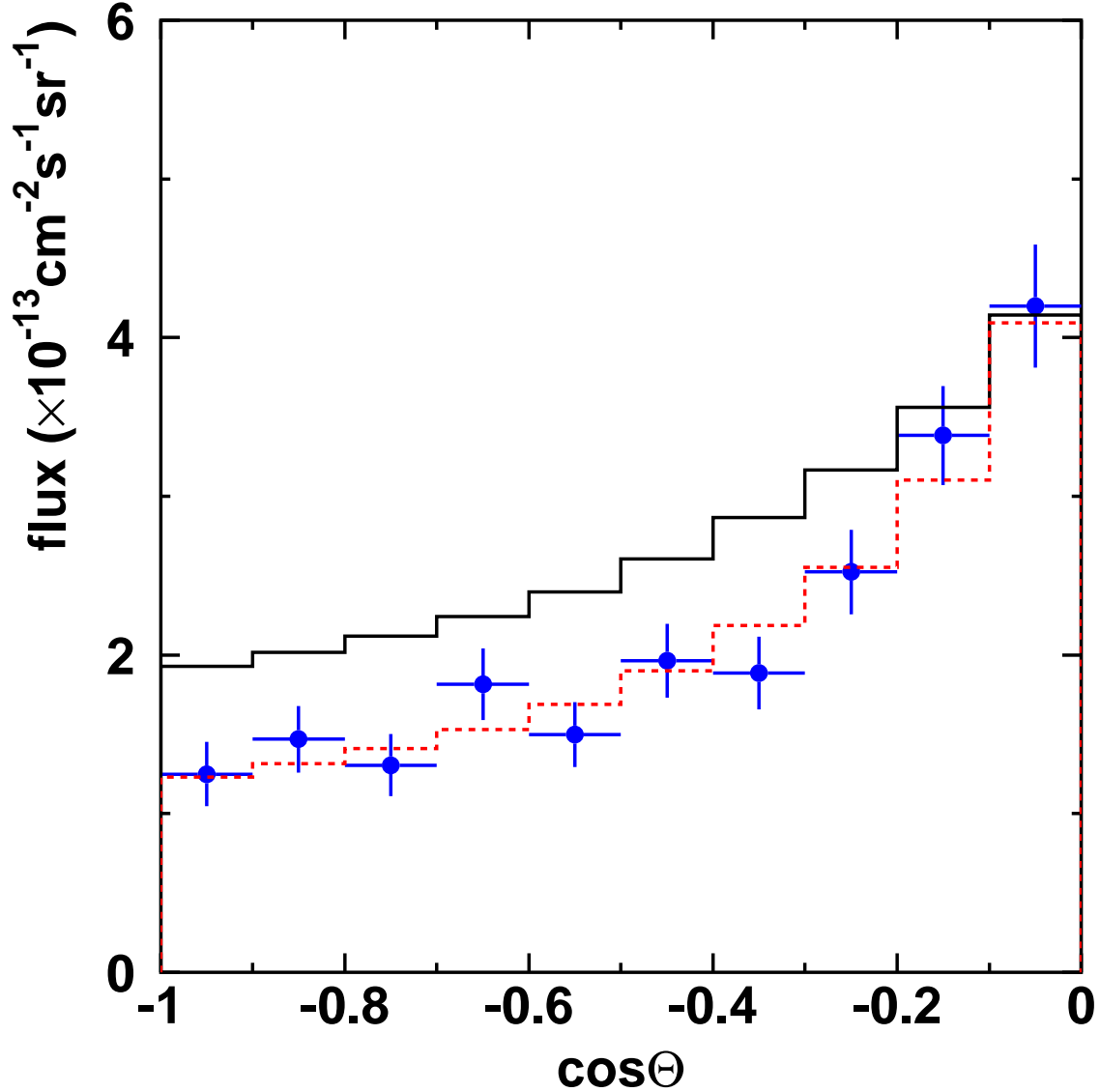


FIG. 5. Upward stopping+through-going muon flux (filled circles) observed in Super-K as a function of zenith angle. The error bars indicate uncorrelated experimental systematic plus statistical errors added in quadrature. The solid histograms show the expected flux based on the Bartol neutrino flux without oscillation. Also shown as dashed histograms are the expected flux assuming the best fit parameters of the combined analysis in the physical region at $(\sin^2 2\theta, \Delta m^2) = (1.0, 3.9 \times 10^{-3} \text{ eV}^2)$, $\alpha = +0.061$ and $\beta = -0.083$ for the $\nu_\mu \leftrightarrow \nu_\tau$ oscillation case.

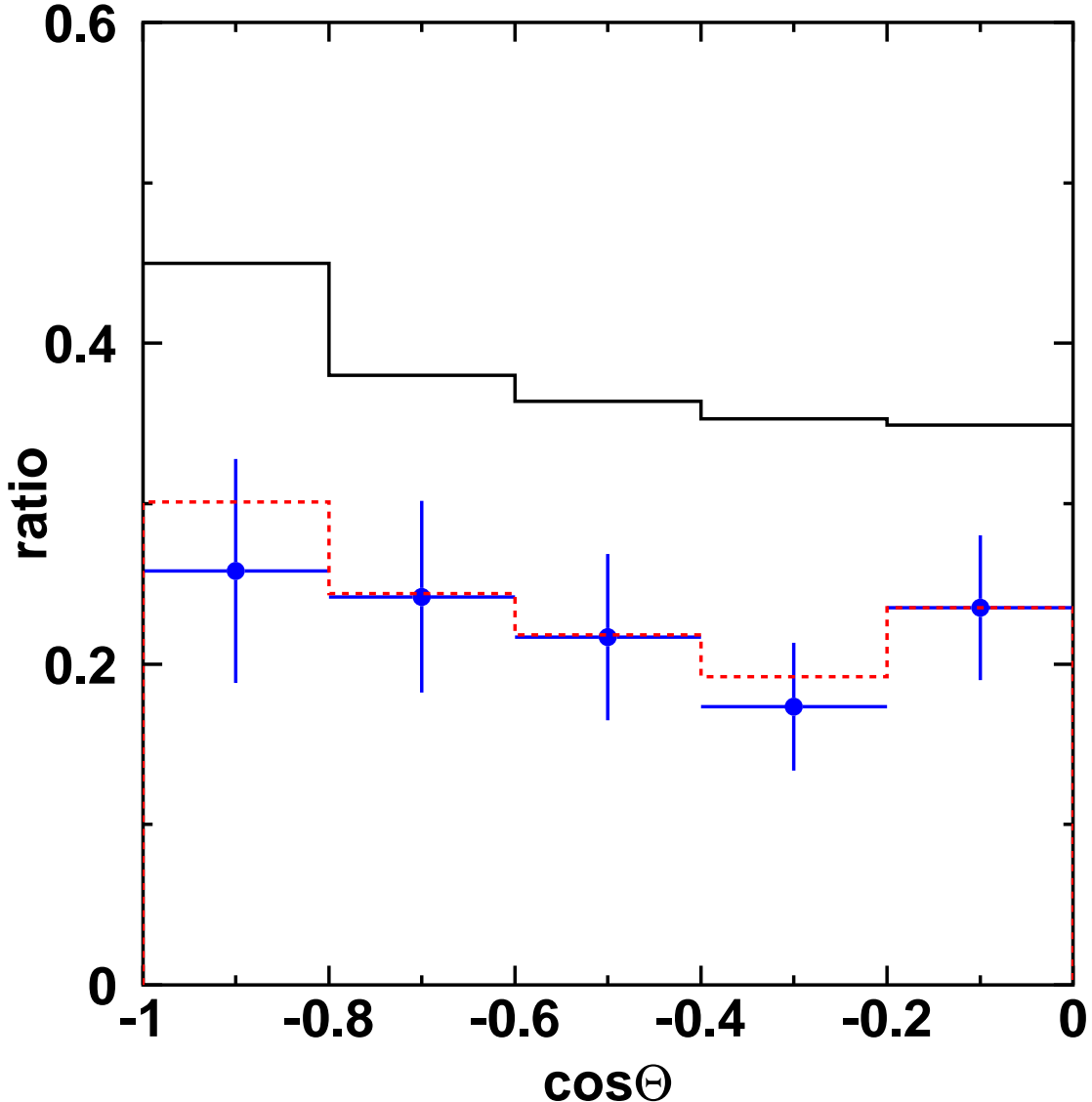


FIG. 6. Upward stopping/through-going muon flux ratio (filled circles) observed in Super-K as a function of zenith angle. The error bars indicate uncorrelated experimental systematic plus statistical errors added in quadrature. The solid histograms show the expected ratio based on the Bartol neutrino flux without oscillation. Also shown as dashed histograms are the expected ratio assuming the best fit parameters of the combined analysis in the physical region at $(\sin^2 2\theta, \Delta m^2) = (1.0, 3.9 \times 10^{-3} \text{ eV}^2)$, $\alpha = +0.061$ and $\beta = -0.083$ for the $\nu_\mu \leftrightarrow \nu_\tau$ oscillation case.

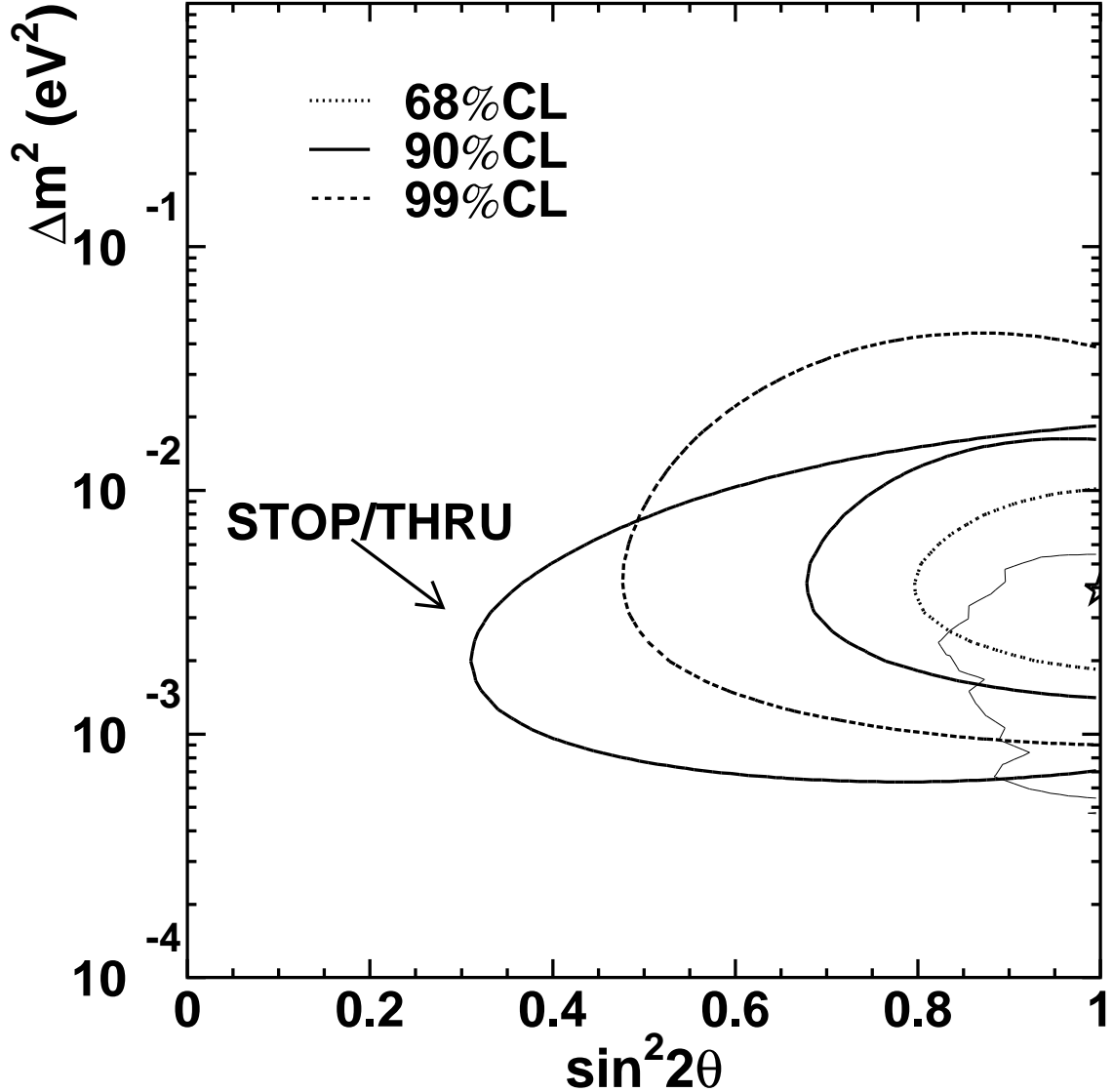


FIG. 7. The allowed region contours at 68% (dotted contour), 90% (thick solid), and 99% (dashed) C.L. obtained by the combined analysis of Super-K upward stopping and through-going muons drawn on the $(\sin^2 2\theta, \Delta m^2)$ plane for $\nu_\mu \leftrightarrow \nu_\tau$ oscillations. The star indicates the best fit point at $(\sin^2 2\theta, \Delta m^2) = (1.0, 3.9 \times 10^{-3} \text{ eV}^2)$ in the physical region. The allowed region contour indicated by solid thick labelled line with "STOP/THRU" is made based on the Super-K stopping/through-going muon ratio alone at 90% C.L. Also shown is the allowed region contour (the remaining solid thin line) at 90% C.L. by the Super-K contained event analysis. The allowed regions are to the right of the contours.

† Deceased

* Supported by the Polish Committee for Scientific Research no. 2P03B05316

‡ Present address: Space Radiation Laboratory, California Inst. of Technology, Pasadena, CA 91125 USA

- [1] Y. Fukuda *et al*, Phys. Rev. Lett. **82**, 2644 (1999).
- [2] Z. Maki, M. Nakagawa and S. Sakata, Prog. Theor. Phys. **28**, 870 (1962); B. Pontecorvo, Sov. Phys. JETP. **26**, 984 (1968).
- [3] Y. Fukuda *et al*, Phys. Lett. **B433**, 9 (1998).
- [4] Y. Fukuda *et al*, Phys. Lett. **B436**, 33 (1998).
- [5] Y. Fukuda *et al*, Phys. Rev. Lett. **81**, 1562 (1998).
- [6] M. Apollonio *et al*, Phys. Lett. **B420**, 397 (1998).
- [7] S. Hatakeyama *et al*, Phys. Rev. Lett. **81**, 2016 (1998).
- [8] M. Ambrosio *et al*, Phys. Lett. **B434** 451 (1998).
- [9] M. Ambrosio *et al*, Astroparticle Physics **9** 105 (1998).
- [10] V. Agrawal, T.K. Gaisser, P. Lipari, T. Stanev, Phys. Rev. **D53**, 1314 (1996).
- [11] C.H. Llewellyn Smith, Phys. Rep. **3**, 261 (1972).
- [12] D. Rein and L.M. Seghal, Ann. Phys. **133**, 79 (1981).
- [13] M. Glück, E. Reya and A. Vogt, Z. Phys. **C67**, 433 (1995).
- [14] W. Lohmann, R. Kopp and R. Voss, CERN Yellow Report No. 85-03.
- [15] M. Honda *et al*, Phys. Rev. **D52**, 4985 (1995), Prog. Theor. Phys. Suppl. **123**, 483 (1996).
- [16] J. Botts *et al*, Phys. Lett. **B304**, 159 (1993); H.L. Lai *et al*, Phys. Rev. **D51**, 4763 (1995).
- [17] W. Frati *et al*, Phys. Rev. **D48**, 1140 (1993).
- [18] R. Becker-Szendy *et al*, Phys. Rev. Lett. **69** 1010 (1992).
- [19] R.M. Barnett *et al.*, “Review of particle properties. Particle Data Group,”, Section “Gaussian Errors–Bounded Physical Region”, Phys. Rev. **D54**, 164 (1996).